Supporting Information

Modulating and optimizing 2D/2D Fe-$Ni_2P/ZnIn_2S_4$ with S vacancy through surface engineering for efficient photocatalytic H_2 evolution

Guanqiong Li,[a] Haiou Liang,[a] Xiaoye Fan,[a] Xiaoling Lv,[c] Xingwei Sun[a,*], Heng-guo Wang[b,*], Jie Bai[a,*]

[a] G. Li, H. Liang, X. Fan, Dr. X. Sun, Prof. Dr. J. Bai

Chemical Engineering College, Inner Mongolia University of Technology, Huhhot, 010051, P. R. China

E-mail: sxw@imut.edu.cn; baijie@imut.edu.cn

[b] Prof. Dr. H. G. Wang

Key Laboratory of Polyoxometalate and Reticular Material Chemistry of Ministry of Education and Faculty of Chemistry, Northeast Normal University, Changchun 130022, P. R. China

E-mail: wanghg061@nenu.edu.cn

[c] Dr. X. Lv

School of Materials Science and Engineering, Changchun University of Science and Technology, Changchun 130022, P. R. China

Experimental

1.1 Synthesis of ZIS

In a representative experiment, $ZnCl_2·2H_2O$ (1.0 mmol), $InCl_3$ (2.0 mmol) and TAA (8.0 mmol) were orderly dissolved into 60 mL ethanol solution (V_{H2O}:$V_{ethanol}$ = 1:1), and then stirred at room temperature for 30 min. Thereafter, the clear solution was poured into 100 mL stainless steel autoclave, and maintained at 180°C oven for 18 h. After cooling naturally to indoor temperature, the sediment was separated by centrifugation, followed by washing with deionized water and ethanol, and drying at 60°C for 12 h. The obtained yellow powder was labelled as ZIS.

1.2 Synthesis of ZIS with rich S vacancies

The preparation process of ZIS with abundant S vacancies was similar to that of ZIS. It was prepared by shortening the solvothermal time. Typically, 1.0 mmol $ZnCl_2·2H_2O$, 2.0 mmol $InCl_3$ and 8.0 mmol TAA were orderly added into 60 mL ethanol solution (V_{H2O}:$V_{ethanol}$ = 1:1), and then stirred at room temperature for 30 min. After that, the mixture was transfer to 100 mL stainless steel autoclave, and kept oven at 180°C for 4 h. In order to compare the performance, three different solvothermal durations (3, 4 and 5 h) were explored. Finally, the precipitate of each sample was separated by centrifugation, and washing with deionized water for several times, then drying at 60°C for 12 h. The obtained yellow powder with the best performance was labelled as ZIS-Vs.

1.3 Synthesis of Ni_2P/ZIS-Vs

The Ni_2P/ZIS-Vs composite photocatalyst was fabricated by a typical hydrothermal method. Firstly, 0.0789 g $Ni(NO_3)_2·6H_2O$ and 0.0330 g red phosphorus (molar ratio of 1:4) were dissolved in 30 mL ethylenediamine and stirred for 30 min until homogeneous. And then 0.18 g ZIS-Vs was added above mixed solution and continuously stirred for 30 min. Finally, the mixed solution was held at 140°C for 12 h in 50 mL Teflon lined stainless steel reactor. After reaction, the powders were collected and washed with distilled water and anhydrous ethanol for several times, and dried at 60°C for 12 h under vacuum condition. The collected powder was named as $10Ni_2P$/ZIS-Vs, where 10 represented the mass ratio of Ni_2P to ZIS-Vs. The Ni_2P loading was x% (x = 5, 10 and 15) and denoted as xNi_2P/ZIS-Vs. Bare Ni_2P powder was also obtained without adding ZIS-Vs. And the sample with best performance was denoted as Ni_2P/ZIS-Vs.

1.4 Synthesis of Fe doping Ni_2P/ZIS-Vs

The preparation process of Fe doping Ni_2P/ZIS-Vs composite was similar to that of Ni_2P/ZIS. It was fabricated by a typical hydrothermal method. In brief, 0.0789 g $Ni(NO_3)_2{\cdot}6H_2O$, 0.0330 g red phosphorus and 10 mg $FeCl_3$ were dissolved in 30 mL ethylenediamine and stirred for 30 min until homogeneous. Then added 0.18 g ZIS-Vs into the mixed solution and stirred another 30 min. Finally, the above solution was put in 50 mL Teflon lined stainless steel reactor and kept at 140°C for 12 h. After the reaction, the powders were gathered and washed by distilled water and anhydrous ethanol for several times, and dried at 60°C for 12 h. The gathered sample was named as 10Fe-Ni_2P/ZIS-Vs, where 10 represented the added mass of $FeCl_3$. A series of the Fe-Ni_2P/ZIS-Vs composites with different contents of $FeCl_3$ (8, 10 and 12 mg) were prepared using the same process. Among them, bare Fe-Ni_2P powder was also obtained without adding ZIS-Vs. And the sample with best performance was denoted as Fe-Ni_2P/ZIS-Vs. Meanwhile, we also prepared different metal ions ($Mn(SO_4)_2$ H_2O, $CoCl_2$, $CuCl_2$) doped with Ni_2P/ZIS-Vs and marked as M-Ni_2P/ZIS-Vs.

1.5 Characterizations

The morphology and microstructure were investigated by SU8010 scanning electron microscope (SEM) outfitted with an energy dispersive X-ray spectrometer (EDS), and JEM-2100 plus transmission electron microscope (TEM). The crystalline and phase information were characterized by Bruker D8 Advance X-ray diffraction (XRD). The chemical states were investigated by Thermo ESCALAB 250 XI X X-ray photoelectron spectroscopy (XPS, monochromatic Al Kα radiation), and the XPS data was calibrated by C 1 s spectrum (binding energy is 284.8 eV). The light absorption property was researched by the PerkinElmer Lambda 750 S UV-vis spectrophotometer using barium sulfate as standard reference. The recombination of photogenerated carriers was tested by F-4600 spectrofluorometer (375 nm excitation wavelength). The secondary cutoff binding energy was measured by AXIS SUPRA X-ray photoelectron spectroscopy with He I as the excitation source. The surface photovoltage (SPV) measurement were carried out on the system consisting of a 500 W Xe lamp source equipped with a monochromator, a lock-in amplifier with a light chopper, a photovoltaic cell, and a computer. The Raman spectra were conducted on LabRAM HR Evolution Raman spectrometer with 325 nm excitation wavelength to analysis the composition. The electron paramagnetic resonance (EPR) measurement was conducted on JEOL JES-FA200 EPR spectrometer with a 9.054 GHz magnetic field. Photoluminescence (PL) spectra were directly measured by a steady state spectrometer (Edinburgh instruments, UK) and a FLs980 lifetime.

1.6 Photocatalytic water splitting for hydrogen evolution

The hydrogen production experiments were performed on a 150 mL quartz reactor (CEL-PAEM-D6, CEAULIGHT, Beijing). Typically, photocatalyst (5 mg) was added into 50 mL solution involving 15% TEOA as sacrificial agent. Prior to exerting light, the reaction system was degassed for 40 min to thoroughly exclude the air and the dissolved oxygen in reaction system. And the system temperature was kept at 6℃ using circulating water. Then the reaction was proceeded under 300 W Xenon lamp (PLS-SXE 300, Beijing) with a 420 nm cut-off filter. The generated hydrogen was analyzed by GC7920-7F2A gas chromatograph (CEAULIGHT, Beijing, N_2 as carrier gas and TCD detector).

1.7 Apparent quantum yield (AQY) test

The apparent quantum yield (AQY) was measured following the same reaction conditions as photocatalytic test except that the incident light was supplied by a 300W Xe lamp equipped with specific band-pass filters to get the desired monochromatic incident wavelength (λ=420 nm). AQY was calculated based on the following equation:

$$\mathrm{AQY} = N_e/N_p \times 100\% = 2MN_Ahc/SPt\lambda \times 100\%$$

where N_e is the number of reaction electrons, N_p is the number of incident photons, M is the number of hydrogen molecules, N_A is the Avogadro constant, h is the Planck constant, c is the speed of light in a vacuum, S is the irradiation area, P is the light intensity, t is the reaction time, and λ is the light wavelength.

1.8 Photoelectrochemical and electrochemical measurements

The electrochemical tests such as transient photocurrent responses and electrochemical impedance spectroscopy (EIS) were performed on the electrochemical workstation (Chenhua, Shanghai) with a standard three-electrode system. The Pt net and Ag/AgCl were the counter electrode and the reference electrode, respectively. The working electrode was prepared as follows: 5 mg catalyst was dispersed into 90 μL ethanol and sonicated for 20 min, and then put 10 μL Nafion and sonicated another 20 min. Then, 20 μL of the above mixed solution was spread it on the surface of FTO (1.0 cm*1.0 cm) and dry at room temperature. The electrolytes used in the tests were all Na_2SO_4 solutions (0.5 mol/L). 300 W xenon lamp was used as light source and 420 nm cut-off filter. The frequency range selected for the EIS test was 0.1 Hz to 1 MHz in the case of real-time open circuit voltage. Mott-Schottky (M-S) plots were collected from -1 to 0.5 V under 5 and10 kHz frequency and 0.01 V amplitude.

1.9 Theoretical calculation

All calculations in this work are performed using the CASTEP code, which was based on density functional theory (DFT) calculations with the plane wave pseudopotential method. Perdew-Burke-Ernzerhof (PBE) functional in the generalized gradient approximation (GGA) was chosen to describe the exchange correlation potential. The Tkatchenko and Scheffler (TS) scheme was used to correct for the influence of van der Waals (vdW) forces. The plane-wave energy cutoff was set to 480 eV. The tolerance of self-consistent calculation was set as 5.0×10^{-5} eV/atom. The maximum displacement below 0.005 Å and maximum force on atoms below 0.1 eV/Å were set as the convergence thresholds in geometry optimization. To avoid interlaminar interactions, a vacuum spacing of 18 Å was applied perpendicular to the slab.

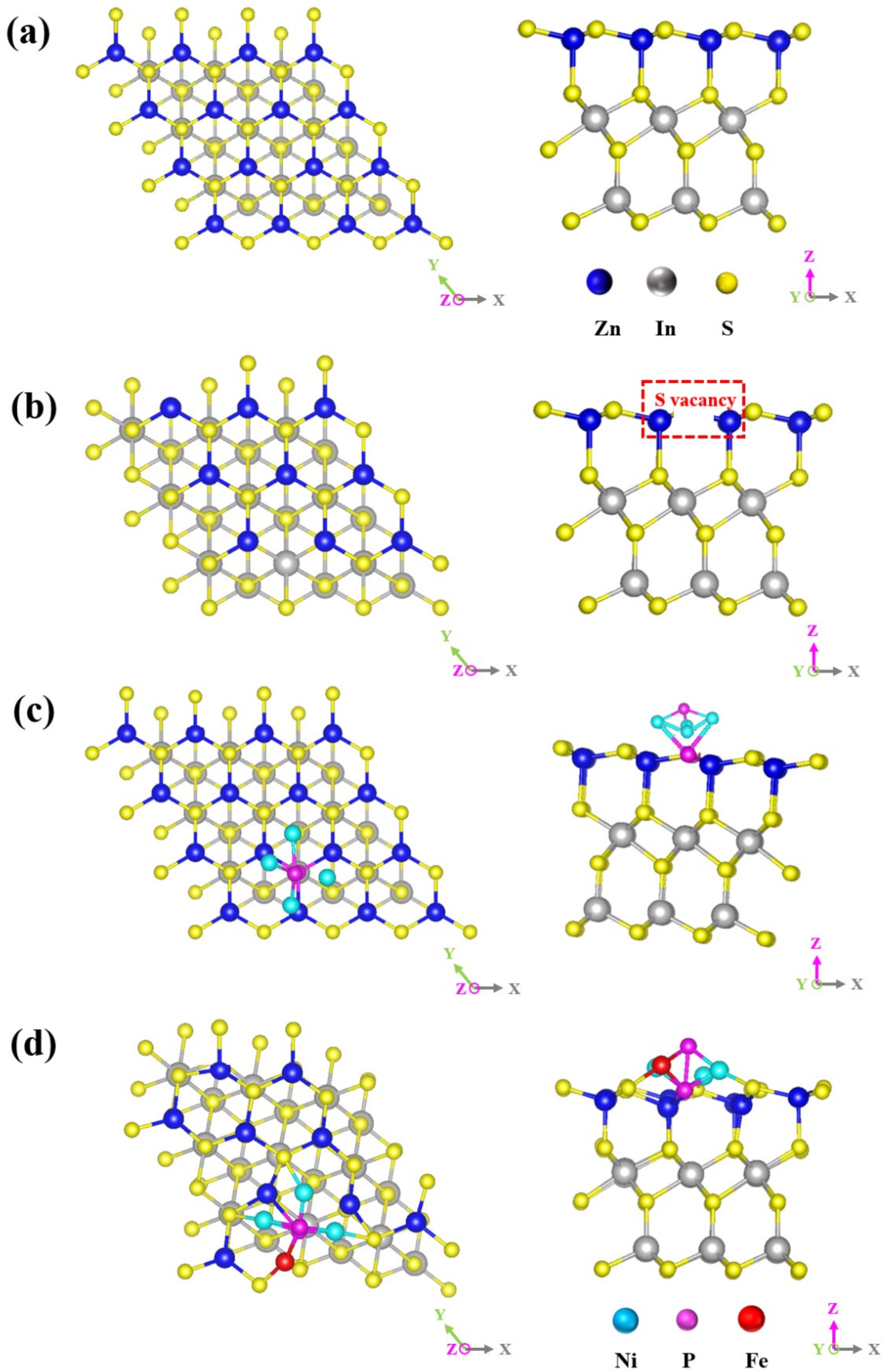

Figure S1. Top-view and side-view models of (a) ZIS, (b) ZIS-Vs, (c) Ni_2P/ZIS-Vs and (d) Fe-Ni_2P/ZIS-Vs used for DFT calculations, dark blue, grey, yellow, light blue, purple and red spheres represented Zn, In, S, Ni, P and Fe atoms, respectively.

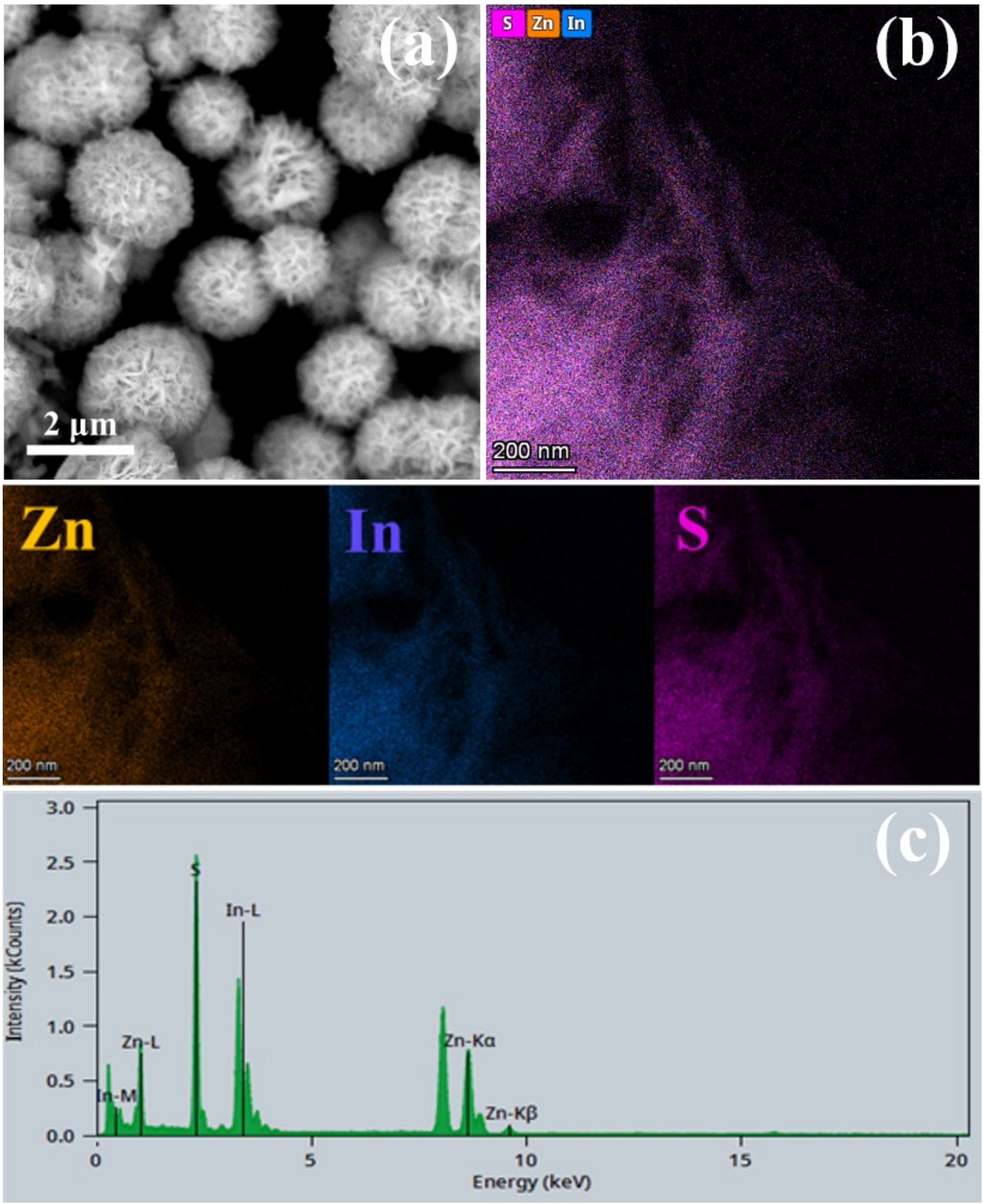

Figure S2. (a) SEM image of pristine ZIS. (b) Elements mappings of Zn, In and S and (c) EDS spectrum of ZIS-Vs.

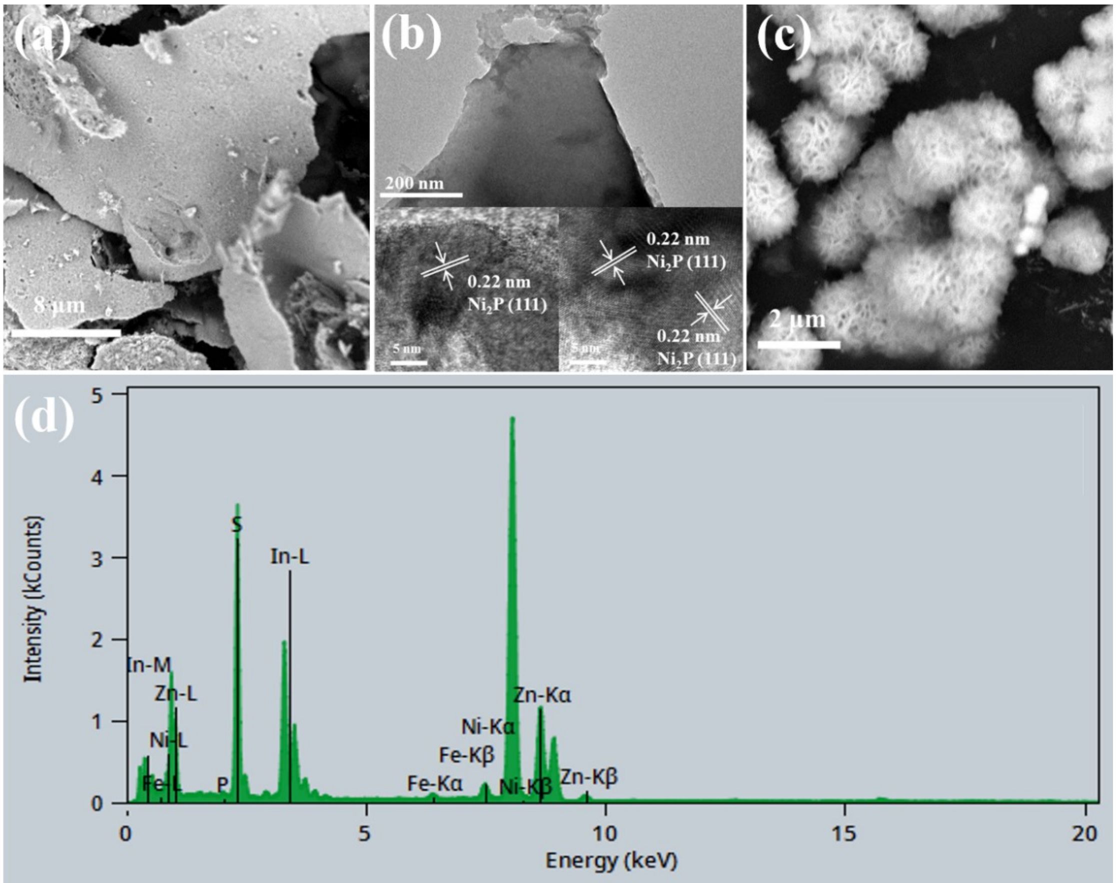

Figure S3. (a) SEM, (b) TEM and HRTEM images of Ni_2P nanoflakes. (c) SEM image of Ni_2P/ZIS-Vs and (d) EDS spectrum of Fe-Ni_2P/ZIS-Vs.

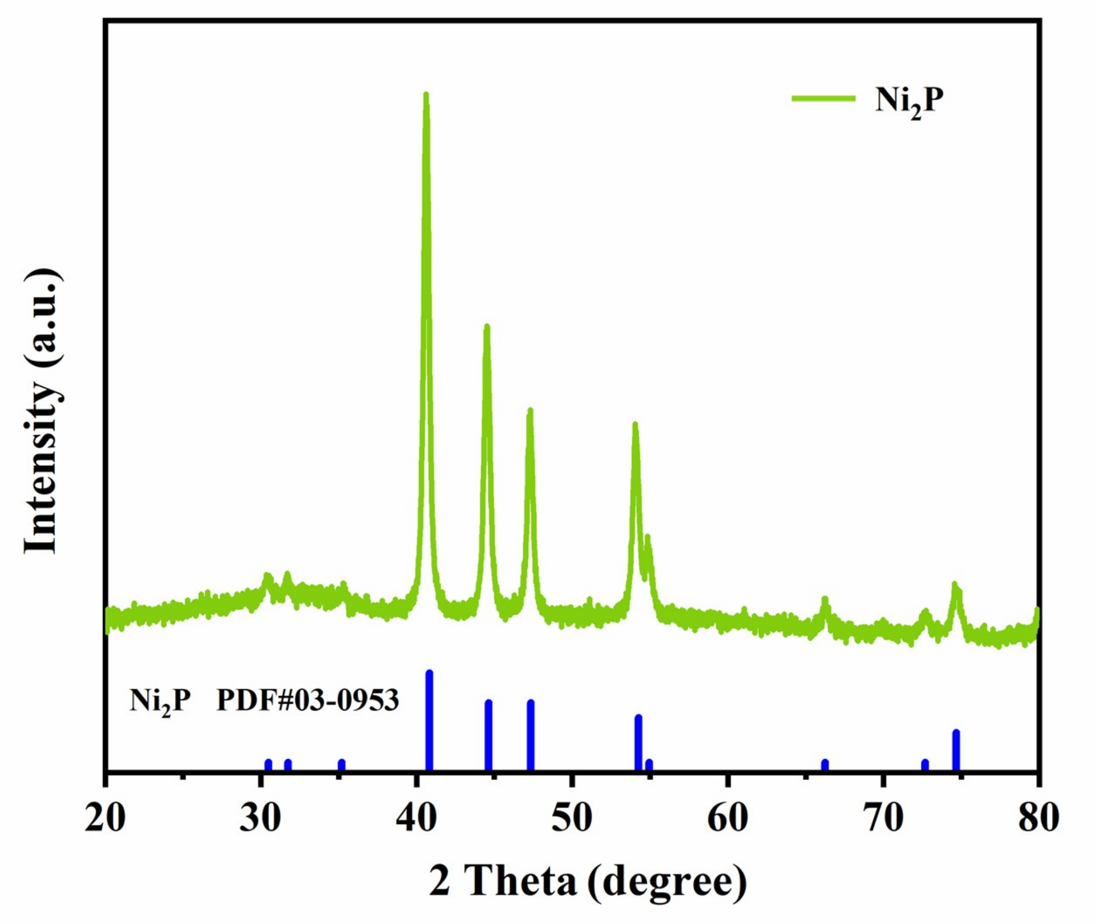

Figure S4. XRD pattern of Ni_2P nanoflake.

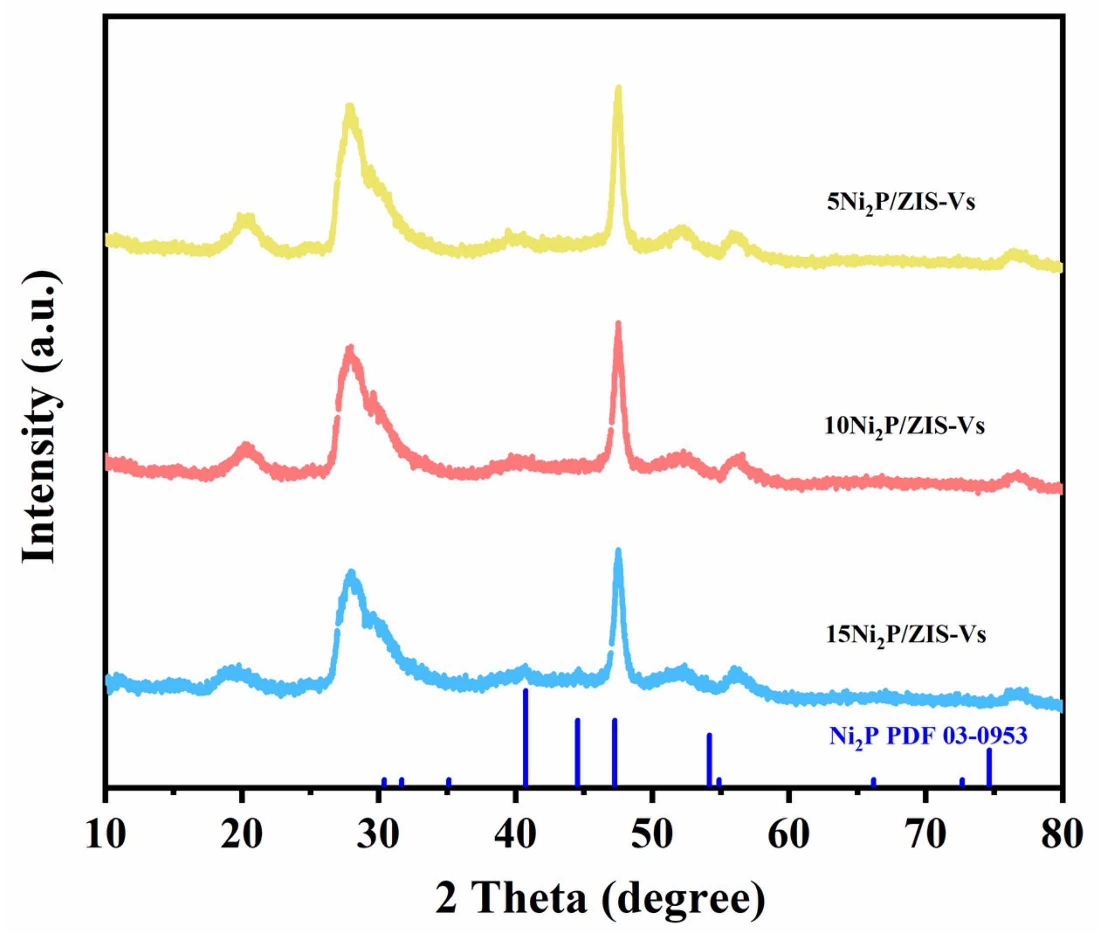

Figure S5. XRD patterns of composite photocatalysts supported with Ni_2P in different proportions.

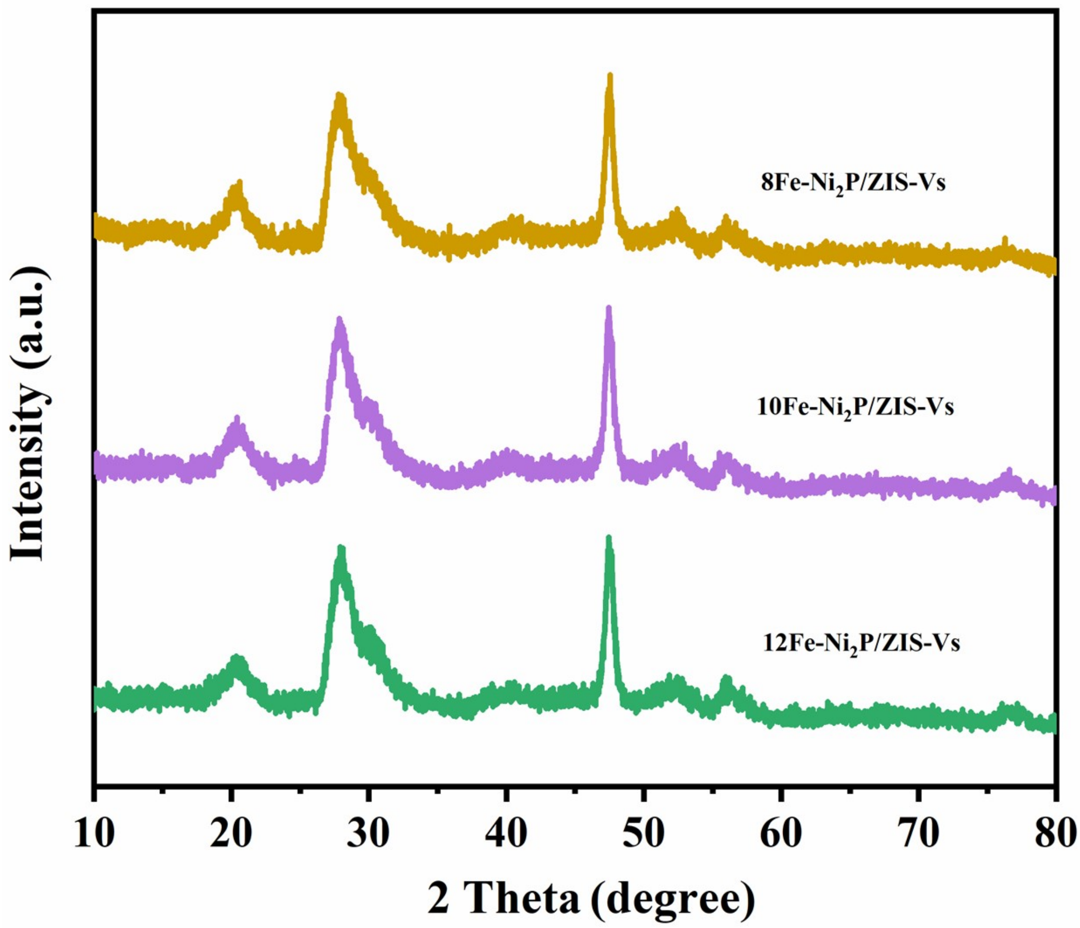

Figure S6. XRD patterns of composite photocatalysts doped with different amounts of Fe element.

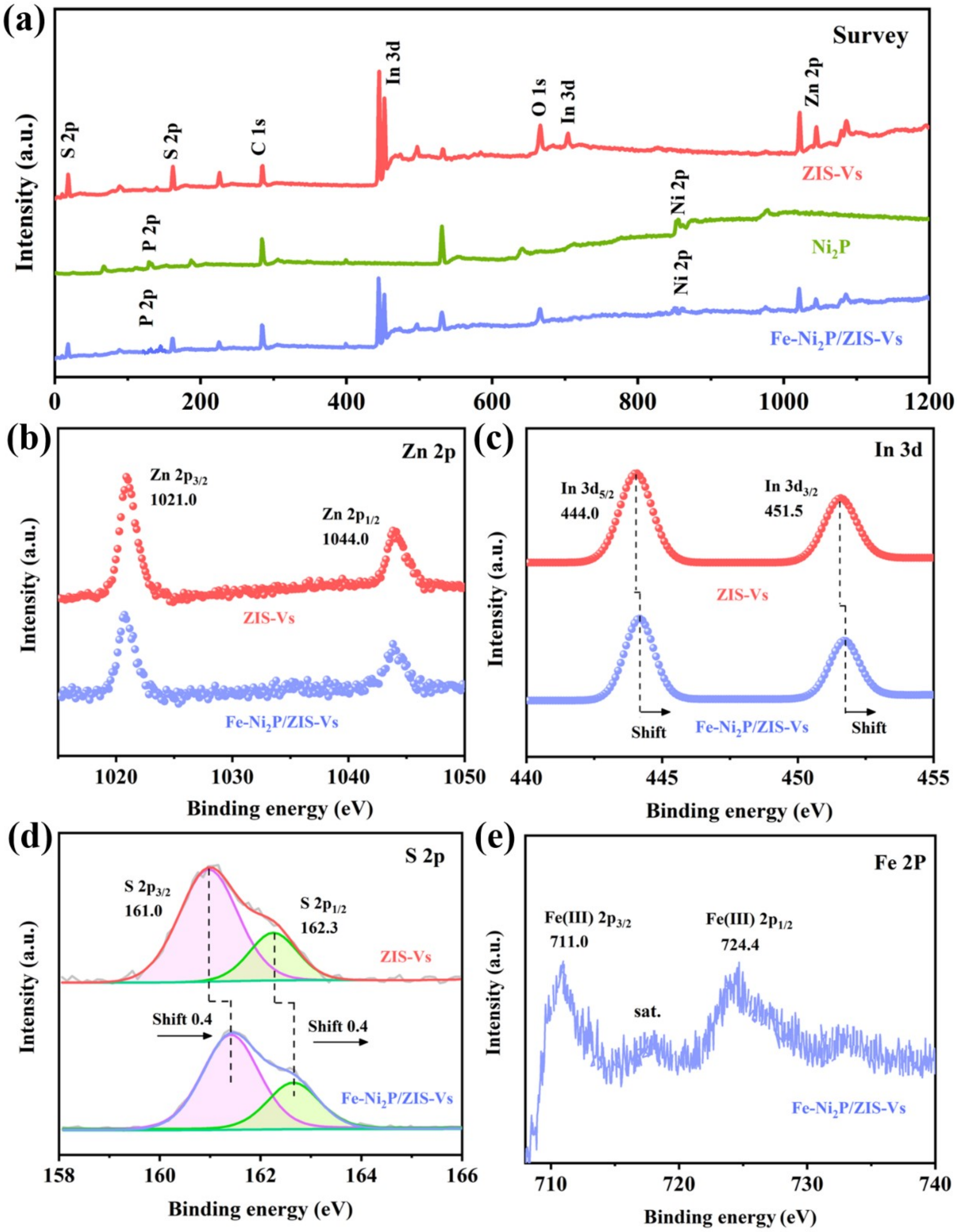

Figure S7. (a) Survey spectra of ZIS-Vs, Ni_2P and Fe-Ni_2P/ZIS-Vs. High-resolution (b) Zn 2p, (c) In 3d and (d) S 2p spectra of ZIS-Vs and Fe-Ni_2P/ZIS-Vs, (e) High-resolution Fe 2p spectrum of Fe-Ni_2P/ZIS-Vs.

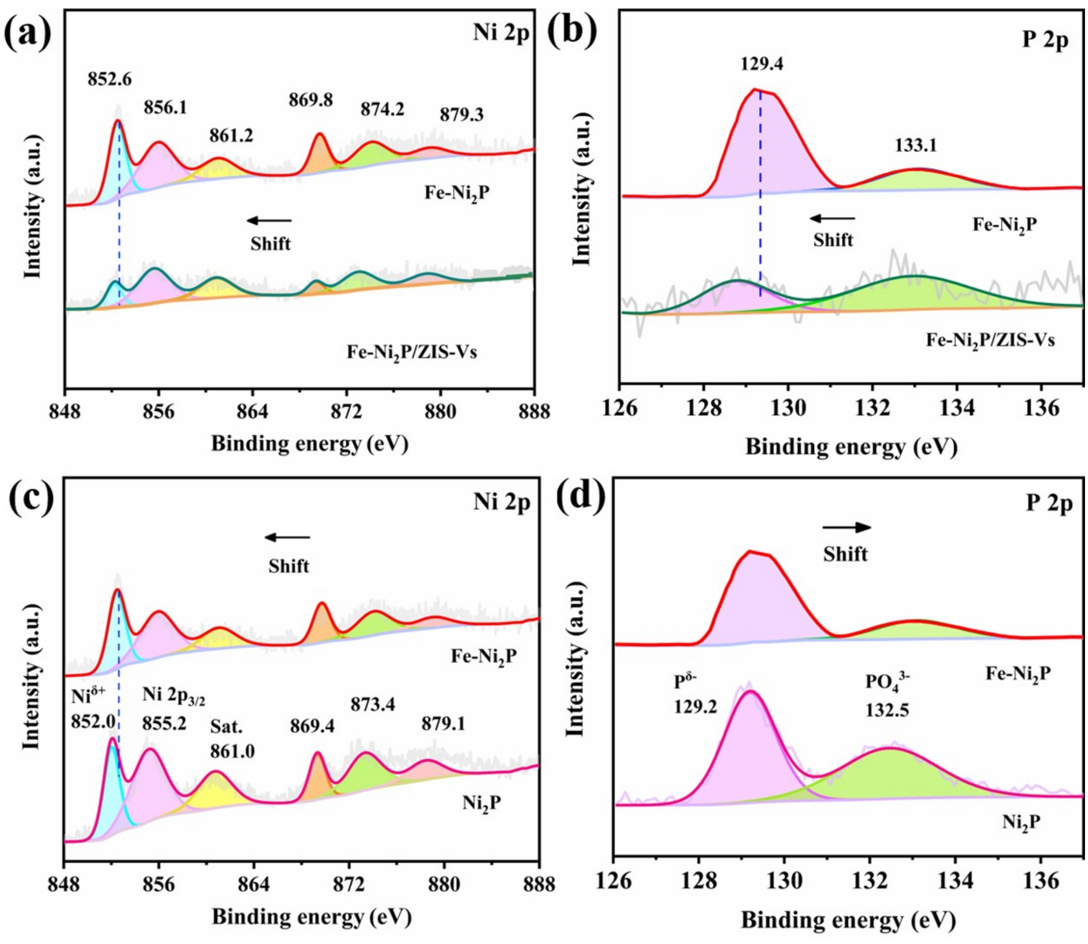

Figure S8. High-resolution (a) Ni 2p and (b) P 2p spectra of Fe-Ni_2P and Fe-Ni_2P/ZIS-Vs. High-resolution (c) Ni 2p and (d) P 2p spectra of Fe-Ni_2P and Ni_2P.

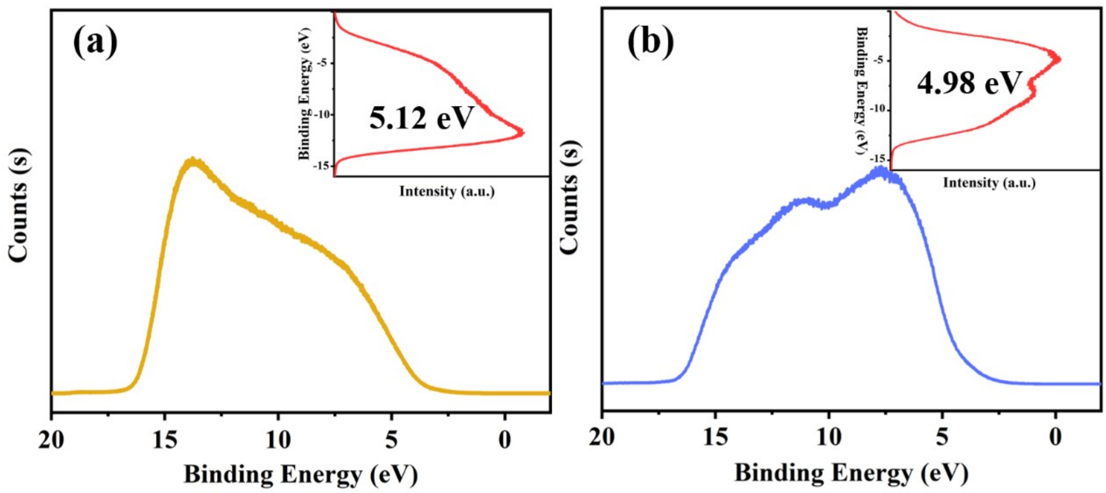

Figure S9. UPS spectra of (a) Ni_2P-ZIS-Vs and (b) Fe-Ni_2P/ZIS-Vs.

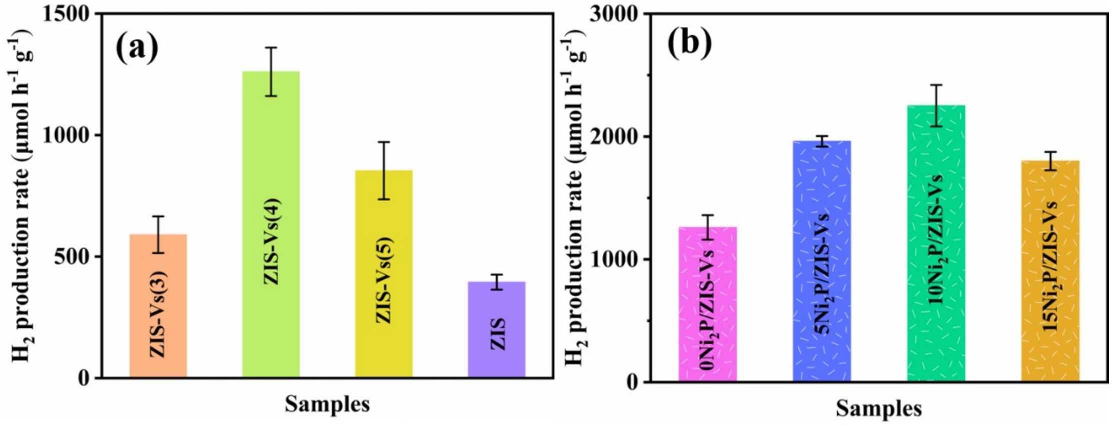

Figure S10. (a and b) The corresponding photocatalytic H_2 evolution rates of various samples.

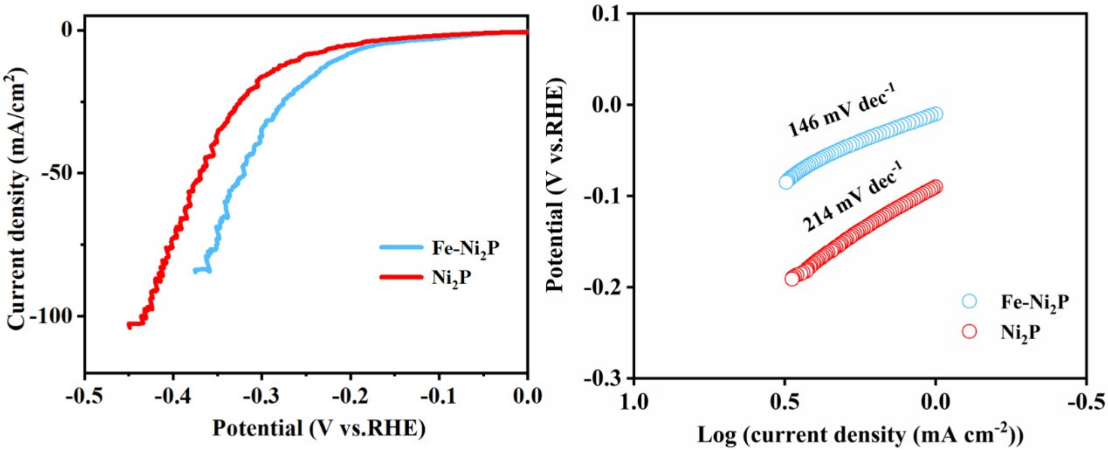

Figure S11. (a and b) The corresponding electrocatalytic hydrogen evolution polarization curves and Tafel plots of samples.

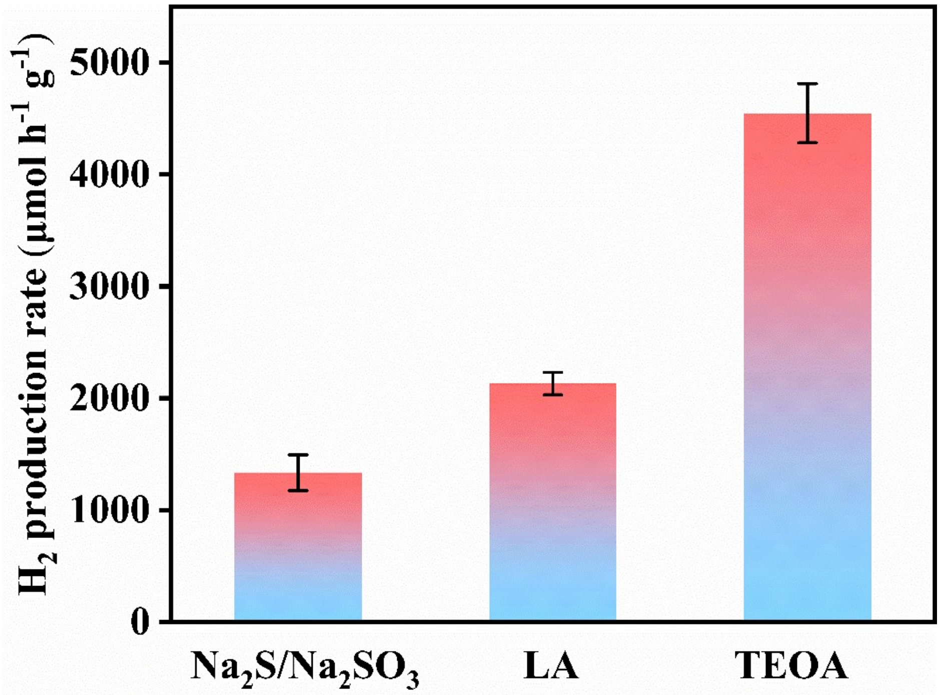

Figure S12. Photocatalytic H_2 evolution rates of Fe-Ni_2P/ZIS-Vs using Na_2S/Na_2SO_3, LA and TEOA, respectively.

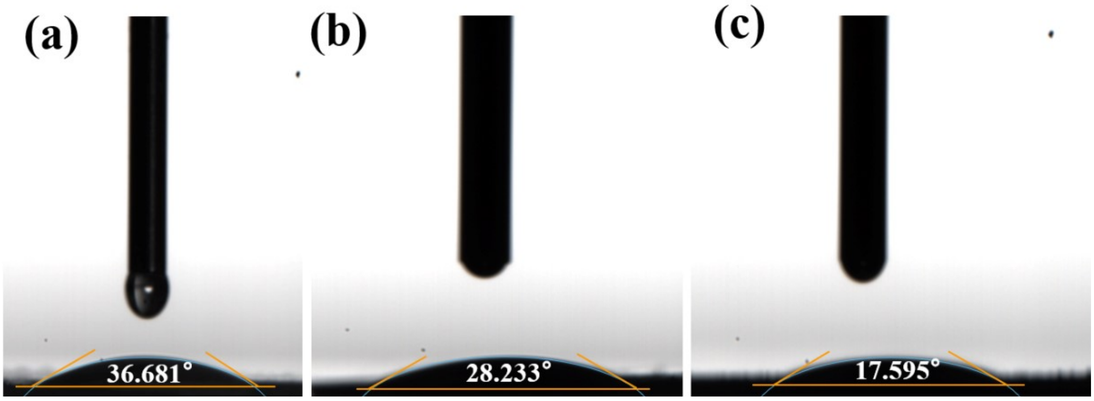

Figure S13. Contact angle measurements of (a) ZIS-Vs, (b) Ni_2P/ZIS-Vs and (c) Fe-Ni_2P/ZIS-Vs.

H_2O adsorption is a key step in photocatalytic reaction for hydrogen production. To better understand the main factors related to the water splitting reaction, it is greatly necessary to research the adsorption property of water molecules. The contact-angle measurements were performed. The pristine ZIS-Vs shows a contact angle of 36.681° (Figure S13a), indicating moderate hydrophilicity. Interestingly, the contact angle of Ni_2P/ZIS-Vs decreases due to the introduction of the cocatalyst Ni_2P (Figure S13b), indicating that Ni_2P induced H_2O adsorption preference. In Figure S13c, the Fe-Ni_2P/ZIS-Vs has the minimum contact angle of 17.30°, which manifests that the dependence of photocatalytic activity on water adsorption is enhanced.

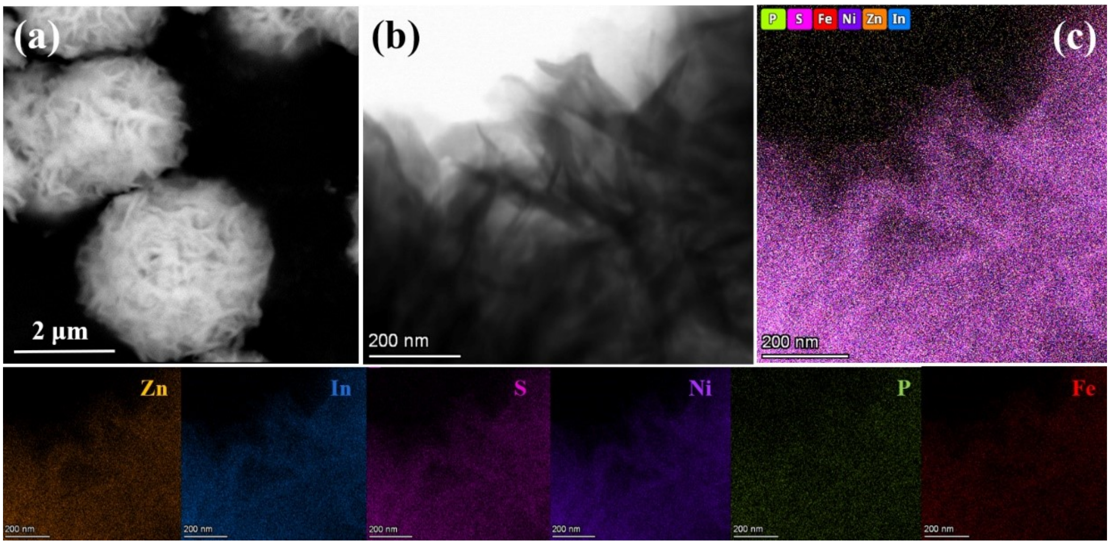

Figure S14. (a) SEM, (b) HRTEM images and (c) elements mapping of recycled Fe-Ni_2P/ZIS-Vs sample.

Table S1. Substrate (E_{sub}), complex (E_{com}), Fe (E_{Fe}) and forming (E_{for}) energies of Fe-Ni_2P/ZIS-Vs with Zn, In or Ni replaced.

Replaced element	E_{sub} (eV)	E_{com} (eV)	E_{Fe} (eV)	E_{for} (eV)
Zn	-59031.10	-58331.09	-856.5	-1.63
In	-59031.10	-58181.13	-856.5	-2.13
Ni	-59031.10	-58541.16	-856.5	-2.36

Table S2. The element atomic fraction of ZIS-Vs.

Element	Zn	In	S
Atomic Fraction (%)	14.86	29.72	55.42

Table S3. The element atomic fraction of Fe-Ni_2P/ZIS-Vs.

Element	Zn	In	S
Atomic Fraction (%)	14.60	29.20	56.20

Table S4. Energy band structures of ZIS-Vs.

Samples	E_g (eV)	E_{fb} vs. Ag/AgCl (V)	E_{CB} vs. NHE (V)	E_{VB} vs. NHE (V)
ZIS-Vs	2.24	-1.07	-1.07	1.17

Table S5. Dynamic analysis of emission decay for ZIS, ZIS-Vs, Ni_2P/ZIS-Vs and Fe-Ni_2P/ZIS-Vs.

Samples	t_1 (ns)	A_1 (%)	t_2 (ns)	A_2 (%)	t_3 (ns)	A_3 (%)	t_{Av} (ns)
ZIS	0.081	97.86	3.219	2.14	0	0	1.54
ZIS-Vs	0.051	97.98	3.409	2.02	0	0	2.00
Ni_2P/ZIS-Vs	0.069	96.84	3.511	3.16	0	0	2.21
Fe-Ni_2P/ZIS-Vs	0.110	85.21	1.531	11.32	11.904	3.47	7.63

Table S6. Performance comparison of $ZnIn_2S_4$-based photocatalysts recently reported.

Samples	Light source	Incident light	Sacrificial agents	H_2/ μmol/g/h	Ref.
S defect $ZnIn_2S_4$	300W Xe	>420 nm	lactic acid/Na_2S	2400	1
Cu-$ZnIn_2S_4$	300W Xe	>420 nm	Na_2S/Na_2SO_3	757.5	2
Mn-$ZnIn_2S_4$	300W Xe	>420 nm	Na_2S/Na_2SO_3	1040	3
Co-$ZnIn_2S_4$	300W Xe	>420 nm	Na_2S/Na_2SO_3	1002	4
$ZnIn_2S_4$/$Ni_{12}P_5$	300W Xe	>420 nm	Na_2S/Na_2SO_3	2263	5
Ni_2P/$ZnIn_2S_4$	300W Xe	>420 nm	TEOA	2066	6
$ZnIn_2S_4$&NiS	300W Xe	>420 nm	Lactic acid	3333	7
MoS_2/Vs-M-$ZnIn_2S_4$	300W Xe	>300 nm	Lactic acid	6884	8
Fe-Ni_2P/$ZnIn_2S_4$-Vs	300W Xe	>420 nm	TEOA	4509.87	This work

References

[1] X.D. Jing, N. Lu, J.D. Huang, P. Zhang and Z.Y. Zhang, *J. Energy Chem*., 2021, **58**, 397-407.

[2] S.H. Shen, L. Zhao, Z.H. Zhou and L.J. Guo, *J. Phys. Chem. C*, 2008, **112**, 16148-16155.

[3] S. H. Shen, J. Chen, X. X. Wang, L. Zhao and L. J. Guo, *J. Power Sour*., 2011, **196**, 10112-10119.

[4] W. H. Yuan, X. C. Liu and L. Li, *Acta. Phys-Chim. Sin*., 2013, **29**, 151-156.

[5] D. Zeng, Z. Lu, X. Gao, B. Wu and W.J. Ong, *Catal. Sci. Technol*., 2019, **9**, 4010-4016.

[6] X.L. Li, X.J. Wang, J.Y. Zhu, Y.P. Li, J. Zhao and F.T. Li, *Chem. Eng. J*., 2018, **353**, 15-24.

[7] A. Yan, X. Shi, F. Huang, M. Fujitsuka and T. Majima, *Appl. Catal. B Environ*., 2019, **250**, 163-170.

[8] S.Q. Zhang, X. Liu, C.B. Liu, S.L. Luo, L.L. Wang, T. Cai, Y.X. Zeng, J.L. Yuan, W.Y. Dong, Y. Pei and Y.T. Liu, *ACS Nano*, 2018, **12**, 751-758.